

Energy relaxation and quenching processes of doped rare-gas clusters with a shell-like geometric structure

T. Laarmann,^{a)} K. von Haeften,^{b)} H. Wabnitz, and T. Möller

Hamburger Synchrotronstrahlungslabor HASYLAB at Deutsches Elektronen-Synchrotron DESY, Notkestr. 85, 22603 Hamburg, Germany

(Received 11 September 2002; accepted 20 November 2002)

Energy relaxation processes of photo-excited Kr_{50} clusters covered with a shell of Ar atoms (up to 40), which are embedded inside large Ne_{7500} clusters are investigated with energy resolved fluorescence spectroscopy. In the energy range of the characteristic Ne cluster absorption (16.5–18 eV) a strong energy transfer to the embedded Kr cluster is observed, which results in the desorption of electronically excited Kr^* atoms. Kr^* atoms move through the Ne cluster, desorb and emit visible and near-infrared light in the vacuum ($5p \rightarrow 5s$). By coating the Kr clusters with Ar atoms, the Kr lines disappear and $4p \rightarrow 4s$ transitions of Ar^* become dominant. Additionally, new emission bands occur, which are assigned to transitions of perturbed atomic Kr $5p$ -states inside Ne clusters. Due to the interaction of electronically excited Kr^* atoms with neutral Ar atoms in the surrounding shell, several excited Kr states namely $5p [1/2]_0$ and $5p [3/2]_2$ decay nonradiatively. This is in agreement with the well-known “energy-gap law.” The results give experimental evidence that clusters with a multishell structure can be prepared by a sequential pick-up technique. This allows the preparation of Kr clusters embedded inside Ne clusters and coated with a shell of Ar atoms. Such clusters cannot be prepared with conventional coexpansion techniques. © 2003 American Institute of Physics. [DOI: 10.1063/1.1536982]

I. INTRODUCTION

Clusters containing from a few to several thousands of atoms or molecules have been investigated intensively in the past in order to study the evolution of the properties of bulk matter from the properties of the single constituents. Here, the electronic structure and dynamics of excited states of clusters has attracted considerably interest particularly with regard to optical and electronic properties. Investigations on doped clusters offer the opportunity to obtain information on the host cluster and the impurity atoms, molecules or radicals, since the excitation is usually localized on the impurity.^{1,2} If large clusters are doped with several atoms or molecules, embedded clusters of the doped material can be formed inside large host clusters.³

In this context rare gas clusters are especially well suited as host material, since they exhibit low chemical reactivity and in addition rare gas clusters are transparent within the vacuum-ultraviolet (VUV) spectral range.⁴ Supersonic free jets of rare gas clusters offer the possibility of probing isolated molecules and complexes at very low temperatures. The results shed light on important issues such as ion solvation and structural metastability. As an example, recent studies on polymers of strongly dipolar molecules, HCN^5 and HCCCN^6 embedded in large helium droplets demonstrate the selective preparation of hydrogen-bounded linear chains, despite the fact that for longer chains, cyclic or antiparallel chains are lower in energy. The size of the linear chain that can be formed, turns out to be precisely limited by the drop-

let diameter. The molecular rearrangement into the lowest energy configuration is suppressed, because of the low He cluster temperature (0.38 K) and the rapid cooling mechanism.⁷ Therefore, doped clusters offer the possibility to study spectroscopic properties of complexes, which are special in many respects.

Upon electronic excitation a nonequilibrium configuration of the electronic and nuclear structure occurs. The electron distribution in the excited site initiates nuclear rearrangements around this site. These structural changes cause nonradiative transitions to lower lying electronic states. Therefore, structural changes and electronic transitions are strongly coupled. Between the fast ($\sim 10^{-16}$ s) electronic excitation process and the radiative decay process that takes place after 10^{-9} s or longer, an interesting cascade of non-radiative electronic transitions and of structural changes take place.⁸ In this context desorption processes of electronically excited atoms or molecules play an important role in the energy dissipation of doped rare-gas solids.⁹ Similar processes were also observed in the relaxation cascade of pure He and Ne clusters as well as in small clusters of heavy rare gases.¹⁰ Here, surface excitons, respectively localized atomic or molecular centers near the surface are of fundamental importance. Modifying surface properties of embedded cluster will certainly influence the desorption process and will provide new insight in the electronic energy dissipation of doped clusters. Thanks to recent progress in the preparation techniques of doped clusters, it is now possible to cover the surface of embedded clusters with a well-defined number of atoms of a third material. These atoms form a shell around the cluster on the inside of large host clusters. This allows

^{a)}Electronic mail: tim.laarmann@desy.de

^{b)}Present address: Ruhr-Universität-Bochum, 4478 Bochum, Germany.

the controlled modification of surface properties of embedded clusters and gives information on hindered desorption processes and in particular on the movement of desorbed, electronically excited atoms in doped clusters with a shell-like structure.

In this article, we present results of Kr and Ar doped Ne clusters, which were investigated with energy resolved fluorescence spectroscopy in the visible and near infrared (VIS/IR) spectral range. In this context a number of questions arise:

- (i) Is the desorption of electronically excited Kr^* atoms from the surface of the embedded cluster hindered due to the influence of Ar atoms in the deposited shell?
- (ii) Are excited atoms caged inside Ne clusters?
- (iii) Which are the main relaxation channels upon Ne cluster excitation leading to energy transfer processes to the embedded Kr cluster and/or to the Ar shell?

The paper is organized in the following way. In Sec. II we describe the experimental set up for investigation of doped clusters. Here, we focus on the preparation of shell-like structures using a sequential pick-up technique. In Sec. III the experimental results are presented. In this chapter we first discuss the case where Ne clusters are either doped with Kr atoms or Ar atoms. The second part focus on embedded Kr clusters, which are coated with a well-defined number of Ar atoms at the surface. In the appendix we explain the method of size determination of embedded clusters in detail.

II. EXPERIMENT

The measurements were performed at the experimental station CLULU at the synchrotron radiation laboratory HASYLAB in Hamburg. The experimental setup which allows the doping of rare gas clusters in a sequential pick-up process with atoms from two cross-jets is described in Ref. 11. In brief, $\text{Ne}_{\bar{N}}$ clusters are prepared in a supersonic expansion through a conical nozzle ($d=200\ \mu\text{m}$ diameter, $\alpha=4^\circ$ opening cone angle). At a nozzle temperature of $T_0=30\ \text{K}$ and a stagnation pressure of $p_0=200\ \text{mbar}$ the average Ne cluster size was determined as $\sim\bar{N}=7500$.¹²⁻¹⁴ The width [full width at half maximum (FWHM)] ΔN of the size distribution is $\sim\bar{N}$. In a first step Kr atoms from a cross-jet (Q1) are picked-up by the Ne cluster and stick to the surface of the cluster. When several atoms are picked-up, the Ne-cluster becomes liquid-like since the sum of collision and binding energy is warming up the cluster. Due to the increased mobility of Kr atoms inside the Ne cluster, small $\text{Kr}_{\bar{K}}$ clusters ($\bar{K}=50$) are formed on the inside of the host Ne cluster.¹⁵ In a second step the $\text{Kr}_{50}\text{Ne}_{7500}$ -system is doped with up to 40 Ar atoms (Q2). Since the flight time of the clusters ($\sim 4 \cdot 10^{-5}\ \text{s}$) is long compared to the recombination time, which is of the order $10^{-8}-10^{-6}\ \text{s}$, we assume in the following that the formation of embedded clusters is finished before the clusters interact with the synchrotron radiation.¹⁶ The geometry of the interaction region and the main parameters are shown in the upper part of Fig. 1. For the pick-up process the interaction potential between host cluster atoms

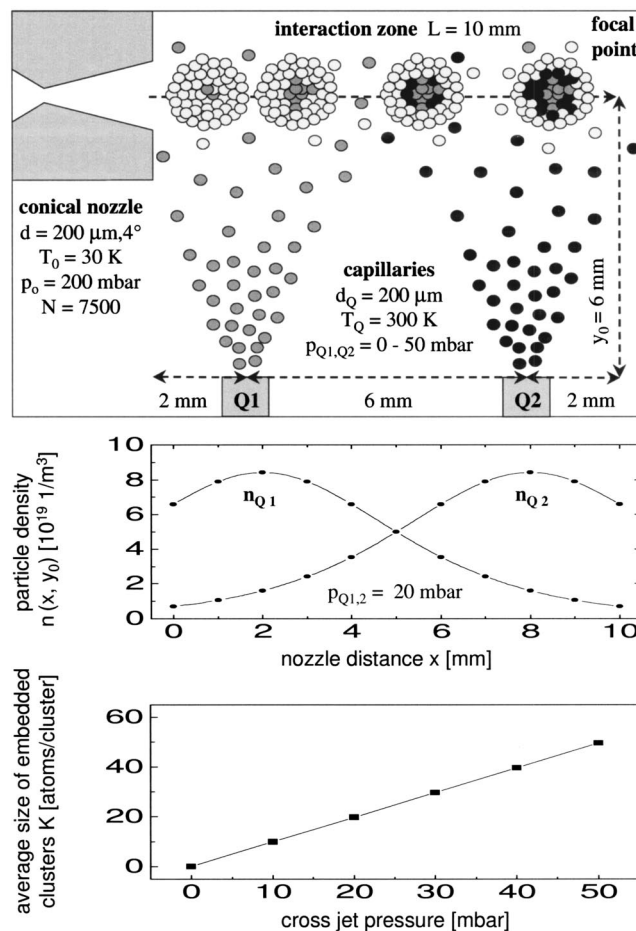


FIG. 1. Upper part: Geometry of the interaction zone including the main parameters; middle part: Ar and Kr particle density distribution along the beam axis; lower part: Calibration curve for average embedded cluster size determination.

and impurity atoms is of fundamental importance. This technique works only, if the binding energy of the cluster atoms is significantly smaller than the interaction between the impurity and the cluster. In Table I we summarized the depth ϵ of different homo- and heteronuclear Lennard-Jones pair potentials.¹⁷ The value $\epsilon' = \epsilon / \epsilon_{\text{Ne-Ne}}$ is a measure of the strengths of different bindings relative to the Ne-Ne interaction. According to the values in Table I, doped Ar atoms in analogy to Kr atoms stick to the Ne cluster surface and penetrate on the inside during the cluster melting. The size determination of the embedded clusters bases on theoretical and experimental work by Lewerenz *et al.*¹⁶ and is explained

TABLE I. Lennard-Jones potential depth ϵ of different homo- and heteronuclear rare-gas molecules (Ref. 17) and $\epsilon' = \epsilon / \epsilon_{\text{Ne-Ne}}$ describing the strengths of different bindings relative to the Ne-Ne interaction.

Molecule	ϵ [meV]	ϵ' [$\epsilon_{\text{Ne-Ne}}$]
Ne-Ne	3.19	1
Ar-Ar	10.34	3.24
Kr-Kr	14.22	4.46
Ne-Ar	5.74	1.80
Ne-Kr	6.74	2.11
Ar-Kr	12.13	3.80

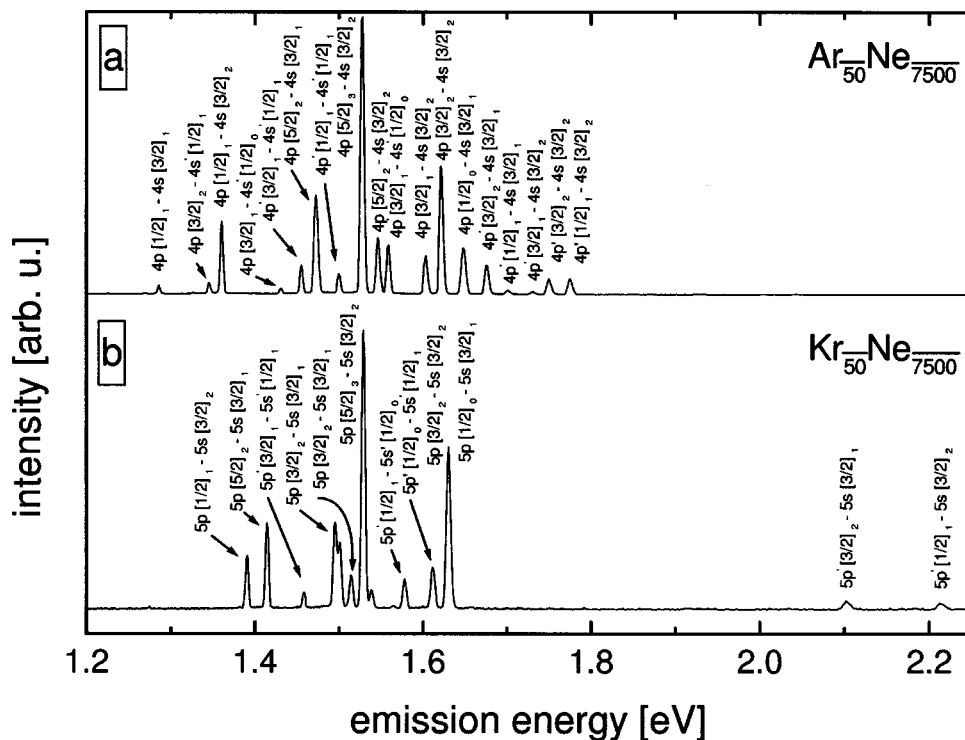


FIG. 2. Energy-resolved VIS/IR fluorescence of doped (a) $\text{Ar}_{50}\text{Ne}_{7500}$ and (b) $\text{Kr}_{50}\text{Ne}_{7500}$ clusters upon excitation of the Ne $11'$ exciton (17.64 eV). Radiative transitions of free Ar^* ($4p, p' \rightarrow 4s, s'$) and Kr^* ($5p, p' \rightarrow 5s, s'$) atoms are indicated Ref. 21.

in the Appendix. According to their work, the average number of picked-up atoms depends mainly on the Ne cluster size and the average particle density of Kr, respectively, Ar atoms, which is a function of the cross-jet pressure. In the middle part of Fig. 1, Kr and Ar particle density distributions $n(x, y_0)$ along the beam axis (x, y_0) are calculated for cross-jet pressures p_Q , temperatures T_Q and capillary diameters d_Q of 20 mbar, 300 K, and 200 μm , respectively.¹⁸ The calculated average size of embedded clusters is shown in the lower part of Fig. 1. We have to point out that all numbers given below are mean values for the cluster sizes. Monochromatized synchrotron radiation (16.5–18 eV) at a resolution of 2.5 \AA (bandpass: ~ 60 meV) was focused 10 mm downstream from the nozzle on the beam. The photo-excited doped clusters emit visible and near-infrared fluorescence light (VIS/IR), which was recorded spectrally resolved with a Czerny–Turner type monochromator and a liquid nitrogen cooled CCD camera. The monochromator is equipped with three gratings (150 l/mm for overview spectra, 1200 l/mm for high resolution). The spectral resolution with the 1200 l/mm gratings is ~ 1 meV and with the 150 l/mm grating ~ 10 meV at 1.5 eV. The monochromator is coupled to the experimental chamber with a lens system consisting of two LiF/Suprasil-achromats in order to minimize chromatic and spherical aberration.

III. RESULTS AND DISCUSSION

It is well-known that pure Ne clusters excited in the energy range of the tightly bound $n=1, 1'$ excitons do not emit VIS/IR photons (the prime denotes the spin orbit state $j=1/2$). Since nonradiative decay to the ground state plays a minor role in condensed rare gases, the energy dissipation process leads mainly to the formation of atomic and molecular self-trapped excitons (a-STE and m-STE), which emit in

the VUV.¹⁹ Whereas these emission bands are dominant in Ne solids, time-resolved VUV emission spectra of Ne clusters show a significant contribution due to the radiative decay of desorbed excited atoms.²⁰ This can be understood taking into account, that clusters exhibit a relatively high fraction of surface atoms and therefore the probability of energy localization near the cluster surface followed by desorption is significantly increased.

On the other hand the energy relaxation pathways change dramatically, if Ne clusters are doped with impurity atoms. In Fig. 2 energy resolved VIS/IR-fluorescence spectra of $\text{Ar}_{50}\text{Ne}_{7500}$ (a) and $\text{Kr}_{50}\text{Ne}_{7500}$ (b) are shown. Here only one of the two cross-jets was used to dope the Ne clusters. The excitation energy was 17.64 eV, which corresponds to the longitudinal branch of the $n=1'$ Ne bulk exciton. The sharp lines in the emission spectra Figs. 2(a) and 2(b) can be assigned to free atomic Ar $p, p' \rightarrow 4s, s'$ and Kr $5p, p' \rightarrow 5s, s'$ transitions.²¹ The energy is transferred from the Ne host cluster to the embedded cluster and localized on excited atomic centers near the surface of the embedded cluster. Due to the repulsive interaction with surrounding neutral atoms, electronically excited Ar^* , respectively Kr^* atoms move through the Ne cluster and emit in the vacuum. This process is similar to exciton induced desorption in pure rare-gas solids.²² In the so-called “cavity-ejection mechanism” the interaction (whether it is repulsive or attractive) is correlated to the sign of the V_0 value (electron affinity) of the respective solid. Detailed investigations show that the correlation not only holds for pure but also for doped materials.⁹ In analogy to pure rare-gas solids the electron affinity is defined: $V_0 := E_g^i - E_{\text{th}}^i$.⁸ Here, E_g^i is the impurity gap energy and E_{th}^i is the threshold energy of impurity-photoelectron emission. A repulsive interaction between the excited atom and the surrounding neutral atoms is expected for positive

TABLE II. Correlation between the V_0 values of pure and doped rare-gas solids (Ref. 8) with the observation of desorption of electronically excited atoms (Ref. 9).

System	V_0 [eV]	Desorption
Ne	+1.3	yes
Ar-Ne	+1.1	yes
Kr-Ne	+1.1	yes
Ar	+0.4	yes
Kr-Ar	+0.3	yes
Kr	-0.3	no

V_0 . In Table II, V_0 is given for different combinations of rare gas impurities and solids. In solid Ar desorbed excited atoms in metastable $4s(3/2)_2$ and $4s'(3/2)_0$ states with kinetic energies of roughly 0.04 eV were observed.²³ Our results show that neon as a rather soft matrix is unable to suppress desorption and to cage excited Ar* atoms. Also in case of Kr doped Ne clusters, the Ne cluster does not cage electronically excited Kr* atoms. To our knowledge, there are no measurements of the kinetic energy distribution of desorbed excited Kr* atoms in small clusters, we could compare our data with.

Interestingly, no VIS/IR emission could be observed upon surface excitation of Ne clusters. According to theory the surface exciton penetration depth is of the order of one mono-layer.²⁴ Therefore, our experimental results give evidence that the embedded clusters are surrounded by more than one mono-layer of Ne atoms because otherwise we should have observed exciton induced energy transfer followed by desorption, respectively, VIS/IR luminescence of free Kr* and Ar* atoms upon surface excitation. In another set of experiments we recorded VUV excitation spectra of embedded clusters.³ The total VUV luminescence yield as a function of the excitation energy is taken as a measure of the cluster absorption, since nonradiative decay to the ground state is inefficient in rare gas clusters.²⁵ In these measurements, we could verify the interpretation of complete solvation, since the characteristic surface absorption bands of embedded clusters disappear due to the influence of the surrounding Ne cluster atoms and contribute to a new interface absorption band.³

The interesting question is now, whether one can slow down the desorption by coating the embedded cluster with an additional material at the surface. To answer this question, we deposited up to $\bar{M}=40$ Ar atoms on the surface of embedded Kr₅₀ clusters. Energy resolved VIS/IR fluorescence spectra of Kr₅₀Ar _{\bar{M}} Ne₇₅₀₀ clusters are shown in Figs. 3(a)–3(c). The spectral resolution is given by the full width half maximum (FWHM) of the sharp atomic lines. The spectra indicate, that the relaxation process is significantly depending on the number of deposited Ar atoms. With forming an Ar shell around the embedded Kr cluster, the following effects are observed:

- (i) $5p, p' \rightarrow 5s, s'$ lines due to transitions of free desorbed Kr* atoms disappear;
- (ii) radiative $4p, p' \rightarrow 4s, s'$ decays of free Ar* atoms become dominant;

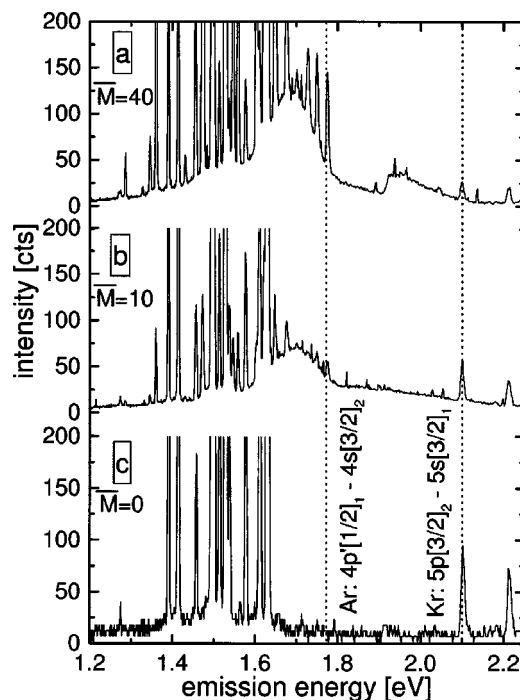


FIG. 3. VIS/IR fluorescence spectra of Kr₅₀Ar _{\bar{M}} Ne₇₅₀₀ clusters with $\bar{M}=40$ (a), $\bar{M}=10$ (b), and $\bar{M}=0$ (c) Ar atoms on the Kr₅₀ cluster surface. As an example the Ar $4p'(1/2)_1 \rightarrow 4s(3/2)_2$ and Kr $5p(3/2)_2 \rightarrow 5s(3/2)_1$ transitions are indicated with dotted lines. The excitation energy was 17.64 eV (Ne 11' exciton).

- (iii) additionally, new broad emission bands in the VIS/IR fluorescence spectra of Kr₅₀Ar _{\bar{M}} Ne₇₅₀₀ ($\bar{M}=10$ and 40) occur, which we interpret as Kr transitions of perturbed atomic $5p, p'$ states inside Ne clusters.

There are two possibilities to interpret the decreased line intensities (Kr), respectively, the increased line intensities (Ar):

- (1) The energy is mainly transferred to the deposited Ar shell;
- (2) the desorption of electronically excited Kr* atoms is hindered.

In the latter case, desorbed excited Kr* atoms are prevented from reaching the Ne cluster surface due to inelastic collisions with Ar shell atoms. To get a deeper insight into the relevant processes it is necessary to analyze the underlying broad structure in more detail. In this context, one has to take into account that recently similar structures were observed in Kr and Ar doped Ne solids.²⁶ Here, the emission bands of embedded Ar and Kr atoms inside the Ne matrix are significantly broadened and shifted relative to the line widths and transition energies of free atoms towards higher energies.²⁶

To check, whether the “sequential pick-up technique” allows the preparation of well-defined cluster shells, we also changed the order of doping. This means as described above, host Ne clusters are first doped with Ar atoms, which form small Ar clusters inside Ne and then interact with Kr atoms from the second cross-jet. In this configuration similar effects to those in Figs. 3(a)–3(c) are observed. But in this case

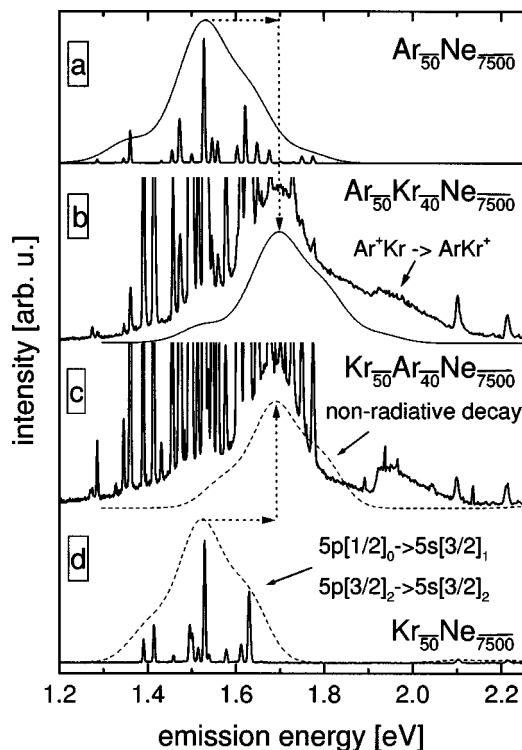


FIG. 4. Energy-resolved VIS/IR fluorescence spectra of doped (a) $\text{Ar}_{50}\text{Ne}_{7500}$, (b) $\text{Ar}_{50}\text{Kr}_{40}\text{Ne}_{7500}$, (c) $\text{Kr}_{50}\text{Ar}_{40}\text{Ne}_{7500}$, and (d) $\text{Kr}_{50}\text{Ne}_{7500}$ clusters upon excitation of the Ne $11'$ exciton (17.64 eV).

$4p, p' \rightarrow 4s, s'$ lines due to transitions of free desorbed Ar^* atoms disappear, while radiative $5p, p' \rightarrow 5s, s'$ decays of free Kr^* atoms become dominant. The experimental findings reinforce our interpretation, since the distribution of atomic lines also carry the information whether Kr clusters are covered by Ar or the reverse. Additionally, new bands again occur, which we interpret as Ar transitions of perturbed atomic $4p, p'$ states inside Ne clusters.

In Figs. 4(a)–4(d) typical fluorescence spectra of photoexcited Ar_{50} and Kr_{50} doped Ne clusters are compared with measurements, where the embedded clusters are coated in a second pick-up process with ~ 40 Kr atoms, respectively, 40 Ar atoms. Concerning the nomenclature, the element which is doped in the first step is named at first. The excitation energy in all measurements was 17.64 eV. Referring to the spectral distribution of nonperturbed Ar and Kr emission [Figs. 4(a) and 4(d)], both shifted ($\Delta E = 168$ meV) and broadened ($\Delta \text{FWHM} = 106$ meV) spectra are included. Perturbed Ar emission is indicated by the solid line, whereas in case of Kr a dotted line is used. Dotted arrows indicate the energy shift. In a crude approximation the polarization energy as well as the exchange interaction of Kr $5p, p'$ and Ar $4p, p'$ electronic states with the surrounding neutral Ne atoms are in the same order of magnitude, since the electronic structure is quite similar. Therefore, it is reasonable to introduce an average energy shift and an average line broadening for both elements. The resulting spectra (solid and dotted line) reproduces qualitatively the shape of the underlying structures for emission energies less than 1.9 eV in case of $\text{Ar}_{50}\text{Kr}_{40}\text{Ne}_{7500}$ clusters and for emission energies less than

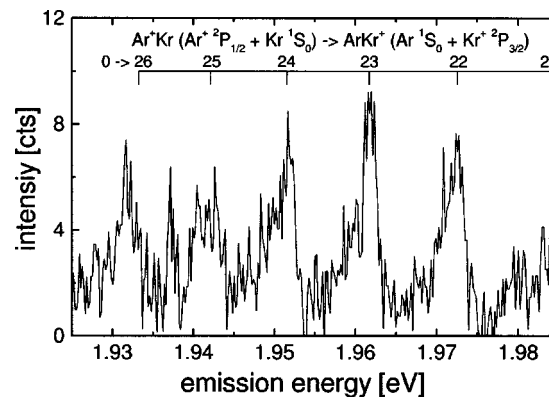


FIG. 5. High-resolution VIS/IR fluorescence of $\text{Ar}_{50}\text{Kr}_{40}\text{Ne}_{7500}$ clusters upon excitation of the Ne $11'$ exciton (17.64 eV). Vertical lines indicate radiative charge transfer transitions $\text{Ar}^+\text{Kr} \rightarrow \text{ArKr}^+ + h\nu$ between different vibrational levels of the molecular ions (taken from Ref. 27).

1.7 eV in case of $\text{Kr}_{50}\text{Ar}_{40}\text{Ne}_{7500}$ clusters. The fact, that the spectral distribution of the VIS/IR fluorescence in Figs. 3(b) and 3(c) is different, if one changes the order of doping is of fundamental importance for the interpretation of the data. It is the experimental proof, that the sequential pick-up indeed allows us to prepare doped clusters with a well-defined shell structure. If we had picked-up atoms from a dilute Ar–Kr gas mixture, the spectra would have looked the same and changing the order of doping should not have influenced the experimental results.

The mismatch between 1.9 and 2.1 eV in case of $\text{Ar}_{50}\text{Kr}_{40}\text{Ne}_{7500}$ in Fig. 4(b) and those between 1.7 and 1.9 eV in case of $\text{Kr}_{50}\text{Ar}_{40}\text{Ne}_{7500}$ in Fig. 4(c) is of different origin, namely charge transfer transitions and nonradiative quenching. This will be explained in the following section.

We have recorded high-resolution spectra in this energy range in order to get additional information. The result is shown in Fig. 5. A sharp vibrational structure is observed, which can clearly be assigned to free atomic Ar $4p, p'$ charge transfer transitions between different vibrational energy levels of the ArKr^+ molecular ions.²⁷ It is not surprising that ionic relaxation channels are involved in the relaxation cascade, since the clusters are excited at 17.64 eV, which is higher than the excited ionic Ar $^2P_{1/2}$ state (15.937 eV). In this sense, the observation of VIS/IR fluorescence of neutral Ar, respectively, Kr is somehow surprising, because the ionization of Ar and Kr should be very effective under these conditions. Therefore, we can conclude, that the excited Ar $4p, p'$ and Kr $5p, p'$ centers are mainly populated due to the recombination of electrons and holes near the embedded cluster surface followed by desorption.

This interpretation is in agreement with results published recently by Belov *et al.*²⁸ They investigated energy relaxation and recombination processes involved in the population of $3p, p'$ centers of Ne solids. They observed a significant increase of the VIS/IR luminescence yield with sample temperature T ($T = 2 - 10$ K), which is explained by the increased mobility of electrons in the solid leading to a more effective population of the recombination channel. The basic mechanism is called dissociative recombination of localized holes with electrons.²⁸ The question to what extent their re-

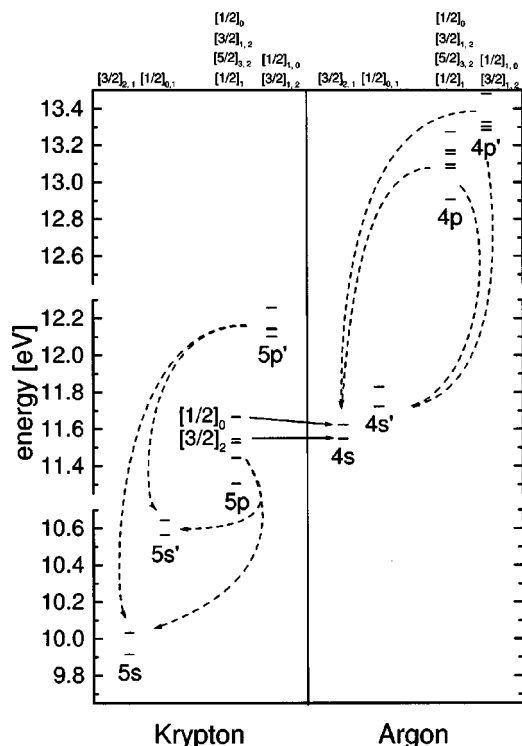


FIG. 6. Term-schemes of electronic states of Kr and Ar atoms. Dotted arrows indicate radiative transitions (Ar $4p$, $p' \rightarrow 4s$, s' and Kr $5p$, $p' \rightarrow 5s$, s'), whereas nonradiative decay processes of $\text{Kr}_{50}\text{Ar}_{40}\text{Ne}_{7500}$ clusters are marked with solid arrows.

sults on pure Ne solids also holds for our measurements on Kr and Ar doped Ne clusters is not easy to answer, since most probably a variety of intermediate excited states are involved in the relaxation cascade and the structures of the corresponding potential surfaces are complicated. Nevertheless, the results give a plausible explanation how neutral fragments might occur.

Coming back to the mismatch in Fig. 4(c) between the broadened and shifted spectrum (dotted line) and the measured VIS/IR fluorescence spectrum of $\text{Kr}_{50}\text{Ar}_{40}\text{Ne}_{7500}$ in the energy range 1.7–1.9 eV. By comparing Fig. 4(c) with Fig. 4(d), one can identify the radiative transitions from perturbed atomic Kr states, which are missing in Fig. 4(c), namely $5p(1/2)_0 \rightarrow 5s(3/2)_1$ and $5p(3/2)_2 \rightarrow 5s(3/2)_2$. Why only these electronically excited Kr states decay nonradiatively and not the corresponding Ar states at about 1.8 eV will be explained in the following. Therefore, we have analyzed the energetic separation of different electronically excited Kr and Ar states in detail. Taking the term schemes of atomic Ar and Kr into account, which are shown in Fig. 6, one gains information on the competition of radiative and nonradiative decay. Since the late sixties, it is well-known that the transition rate of nonradiative decay processes W_{if} in the limit of low temperatures ($T \rightarrow 0$) shows an exponential dependence on the energy difference ΔE_{if} of states i and f involved in the relaxation process. This dependence is called in general the “energy-gap law”^{29,30}

$$W_{if} = W_{if}(T \rightarrow 0) \cdot \exp\left(-\alpha \cdot \frac{\Delta E_{if}}{\hbar \cdot \omega_{\text{ph}}}\right). \quad (1)$$

Here, $W_{if}(0)$ is constant for $T \rightarrow 0$ and describes the electronic transition matrix element as well as the coupling of the electronic states to the lattice. The typical phonon energy is given by $\hbar \cdot \omega_{\text{ph}}$ and α denotes an element specific factor depending on the coupling. The term scheme in Fig. 6 shows, that excited Kr $5p(1/2)_0$ and $5p(3/2)_2$ states have a strong electronic overlap with Ar $4s(3/2)_{2,1}$ energy levels. For example, the energy difference between the excited Kr $5p(1/2)_0$ state and the excited Ar $4s(3/2)_1$ state is less than 43 meV, which is slightly above the Debye energy of rare-gas solids.³¹ Therefore, the high probability of nonradiative decay of these specific states can be understood qualitatively using the “energy-gap law.” Our picture neglects, that the electronic structure of excited Kr^* atoms, which are caged inside Ne clusters, as well as the electronic structure of deposited Ar shell atoms will be significantly changed due to the influence of neighboring atoms. Although this is a crude approximation, the model explains why one specific band in the VIS/IR fluorescence spectrum of $\text{Kr}_{50}\text{Ar}_{40}\text{Ne}_{7500}$ clusters is missing [Fig. 4(c)], where in $\text{Ar}_{50}\text{Kr}_{40}\text{Ne}_{7500}$ clusters it is present [Fig. 4(b)].

Since, the distributions of atomic lines in Figs. 3(a)–3(c), respectively, in Figs. 4(b) and 4(c) also carry the information whether a krypton cluster is covered by argon or the reverse, we analyzed the fluorescence spectra in more detail. In order to obtain additional information about the hindered desorption process, we plotted the fraction of electronically excited Kr^* atoms, reaching the Ne cluster surface and emitting in the vacuum as a function of Ar atoms (\bar{M}) coating the embedded Kr cluster surface.³² Therefore, we integrated the line intensities of the free Kr $5p$, $p' \rightarrow 5s$, s' emission. The same analysis was also performed for the reverse order of doping. The results, depending on the number \bar{M} of coating Ar atoms (closed circles), respectively \bar{K} of Kr atoms (open circles) are presented in Fig. 7. Approximately, the shielded surface of the embedded cluster, from which desorption is hindered, is proportional to the average number of deposited atoms in the second pick-up phase. The general trend of the experimental data fits with the linear functions $f_{\text{Ar}}(\bar{M})$ and $f_{\text{Kr}}(\bar{K})$. From the extrapolation we derive the average number of Ar atoms $\bar{M}_C = 68$, respectively, Kr atoms $\bar{K}_C = 49$ needed for a complete caging. In other words, for $\bar{M} > \bar{M}_C$ and $\bar{K} > \bar{K}_C$ the desorbed electronically excited atoms do not reach the Ne cluster surface and the fraction of free atomic emission in Fig. 7 is equal to zero. Since Ar atoms are smaller and lighter compared to Kr atoms, the suppression of the desorption process is less effective and more Ar atoms are needed to cover the surface completely ($\bar{M}_C > \bar{K}_C$). Therefore, the slope of the experimental data and the $f_{\text{Ar}}(\bar{M})$ function in Fig. 7 is smaller. We would like to note, that the number of atoms is significantly smaller than a complete cover layer for clusters containing ~ 50 atoms. It is well known, that small Ar and Kr clusters have polyicosahedral structures with fivefold symmetry.³³ The clusters (Rg_N) exhibit closed shells with increased stability for $N = 13, 55, 147, \dots$ atoms/cluster (“magic numbers”),³⁴ meaning that 92 atoms are necessary for a complete coverage of the

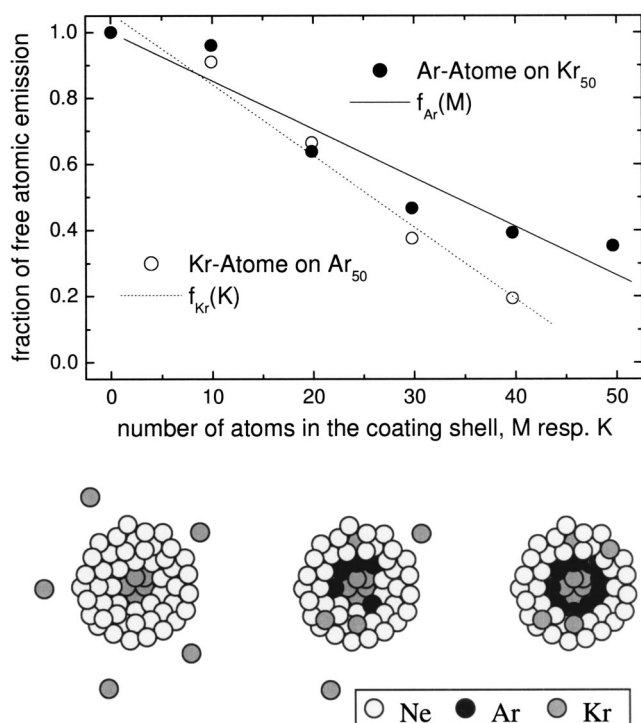


FIG. 7. Fraction of free Kr- (solid circles) and Ar- (open circles) transitions ($5p, p' \rightarrow 5s, s'$ and $4p, p' \rightarrow 4s, s'$) after photoinduced desorption (Ref. 32). The figure includes linear fits f_{Ar} and f_{Kr} of the experimental data (solid and dotted lines).

surface of Rg_{55} . The experimental results in Fig. 7 show that less atoms than in the simple picture of closed icosahedral shells are necessary to suppress the desorption of underlying atoms. A possible explanation could be the following. In the built-up process of small embedded clusters inside large cold Ne clusters (~ 10 K)³⁵ the molecular rearrangement into the lowest energy configuration is suppressed. As mentioned above, similar effects were observed in doped He droplets.^{5,6} Therefore, it could be possible, that in case of embedded Rg_{55} each atom deposited in the second pick-up phase localizes on the center of the 60 triangular faces, which is a local minimum on the associated potential curve. If we further assume, that *one* atom in the cover layer hinders the desorption of up to *three* underlying atoms, we can explain the reduced number of coated atoms needed to build a shell-like structure. On the other hand, we cannot exclude that the desorption rate of electronically excited atoms decreases, because the excitation “gets stuck” in the cover layer, respectively, the branching ratio between energy localization–relaxation within the cover layer and energy transfer to the embedded cluster changes with increasing thickness of the surrounding shell.

To sum up, we can describe our experimental results in the following picture. Electronically excited Kr^* atoms desorb from the surface of embedded Kr clusters. Due to inelastic collisions with deposited Ar atoms in a shell around the Kr cluster, Kr^* are hindered to reach the Ne cluster surface and emit VIS/IR light from perturbed atomic $5p, p'$ states inside Ne. Because Kr $5p(1/2)_0$ and $5p(3/2)_2$ states are depopulated very efficiently (nonradiative decay), the corre-

sponding fluorescence is significantly suppressed for caged Kr^* atoms. Something similar happens, if the order of doping is changed except for the nonradiative decay of electronically excited Ar states. Here, the quenching of specific Ar energy levels is not observed, since the electronic overlap with excited states of Kr shell atoms is small. In particular the difference in the broad underlying structure of Figs. 4(b) and 4(c) shows, that indeed an energy transfer to the embedded cluster for each configuration is observed. Concerning the branching ratio we cannot make a precise statement, because of the variety of intermediate states which take probably part in the relaxation cascade and their complicated potential surfaces. On the other hand excited atoms either Ar^* , respectively, Kr^* , which desorb from the coated shell reach the Ne cluster surface and emit in the vacuum, since Ne is a rather “soft cage.”

Last but not least, we would like to mention that depositing an Ar shell around the embedded Kr cluster is interesting for different reasons. First of all, this is a unique geometric structure, which cannot be prepared using other techniques, like supersonic coexpansion of a dilute Ar–Kr gas mixture through a nozzle or doping free Kr clusters with Ar atoms from a cross-jet. In the former case, single Kr atoms penetrate inside Ar clusters or serve as a condensation nucleus for Ar clusters. The idea to use gas mixture with large Kr concentration does not work out, since here the preparation of pure Kr clusters is favored. This can be understood taking the interaction potentials of Table I into account. For energetic reasons Ar atoms do not stick to the surface of Kr clusters and this also explains why the pick-up technique using free Kr clusters as a host is not possible. On the other hand, we demonstrate the possibility to prepare structural isomers in doped clusters with a “sequential pick-up technique” and to characterize them with fluorescence spectroscopic methods. Secondly, the recent progress in experimental techniques allows the investigation of chemical reactions inside large clusters by adding a third material.³⁶ The large cluster, which serves as a reaction medium, has many degrees of freedom and can, therefore, be considered as a good thermostat as long as the reactants stay in contact with the cluster. The use of different host cluster materials allows the study of condensation and quenching reactions at different temperatures, ranging from ~ 0.4 K in He, ~ 10 K in Ne and ~ 32 K in Ar clusters, respectively.^{35,37} Further advantages are of course first the possibility of controlled surface or bulk localization of a finite number of reactants and second the finite size of the reaction medium.

IV. CONCLUSION

The energy dissipation of photo-excited Kr and Ar doped Ne clusters is investigated with energy-resolved VIS/IR-fluorescence spectroscopy using monochromatized synchrotron radiation. The study of desorption processes of excited atoms and in particular the cage effect and quenching processes in clusters with a shell-like geometric structure were of special interest.

The measurements show, that in the case of Kr doped Ne clusters the energy transfer leads to the desorption of electronically excited Kr^* atoms. The atoms move through the

Ne cluster, desorb and emit VIS/IR-light in the vacuum. The results indicate that Ne is a rather soft matrix which is unable to suppress desorption by caging the excited Kr* atoms.

By coating the embedded Kr cluster in a second pick-up process with up to ~ 40 Ar atoms, the Kr lines disappear and atomic Ar transitions become dominant. Additionally, new bands occur, which are assigned to transitions of perturbed atomic Kr states inside Ne clusters. In this picture, desorbed excited Kr* atoms are prevented from reaching the Ne cluster surface by inelastic collisions with the Ar shell atoms. The interpretation of the experimental results is confirmed by changing the order of doping (first Ar then Kr). Additionally, we observed nonradiative decay of several electronically excited Kr states [$5p(1/2)_0$ and $5p(3/2)_2$], when the embedded Kr cluster is coated with Ar atoms at the surface. This can be understood taking the strong electronic overlap with Ar $4s(3/2)_{2,1}$ energy levels into account.

Using the stepwise pick-up technique we successfully formed a shell of Ar atoms around Kr clusters, which is not possible using other techniques, e.g., coexpansion of a dilute Ar–Kr gas mixture. The host Ne cluster is important to stabilize this special geometric structure.

ACKNOWLEDGMENTS

We thank Professor G. Zimmerer (University of Hamburg) and Dr. P. Gürtler (HASYLAB) for very helpful discussions. The financial support for this work was provided by the Deutsche Forschungsgemeinschaft under the Grant No. Mo719/1-3 and is gratefully acknowledged.

APPENDIX: SIZE DETERMINATION OF EMBEDDED CLUSTERS

The probability P for a Ne cluster (capture cross section σ_{cap}) passing through the interaction zone (length L and average particle density \bar{n}_S) and picking up k atoms is described by the Poisson-statistics¹⁶

$$P_k(L) = \frac{(\sigma_{\text{cap}} \bar{n}_S L)^k}{k!} \cdot \exp[-\sigma_{\text{cap}} \bar{n}_S L]. \quad (\text{A1})$$

The cross-jet particle density along the cluster beam axis (x, y_0) for cross-jet pressures p_Q , temperatures T_Q and capillary diameters d_Q is given by¹⁸

$$n(x, y_0) = C_1 \cos^2(C_2) \cdot \cos^2\left[\frac{\pi}{2\Phi} \cdot C_2\right], \quad (\text{A2})$$

$$\text{with } C_1 = \frac{Z_p d_Q^2 p_Q}{y_0^2 k_B T_Q} \text{ and } C_2 = \arctan\left(\frac{x - x_0}{y_0}\right).$$

In this equation $Z_p = 0.157$ and $\Phi = 1.365$ are numerical constants for rare gases.¹⁸ x_0 denotes the x coordinate of the cross-jet position and k_B is the Boltzmann constant. The average particle density \bar{n}_S is simply

$$\bar{n}_S = \frac{1}{L} \cdot \int_0^L n(x, y_0) dx. \quad (\text{A3})$$

In a crude approximation, we assume that the sum of the Ne \bar{n} cluster cross section and the atomic cross section is equal to the capture cross section. Monte Carlo simulations and ex-

periments on the scattering and capture cross section of He clusters show that the effective geometric cross-section σ_{geo} for light atoms (e.g., Ar) or large He \bar{n} clusters ($\bar{N} > 3000$) is in good agreement with the measured capture cross-section σ_{cap} .^{16,38} In the case of Ar doped He \bar{n} clusters Lewerenz *et al.* obtained for the so-called “sticking coefficient” a value of $s = \sigma_{\text{cap}} / \sigma_{\text{geo}} \approx 0.94$.^{16,38} In this approximation we get

$$\sigma_{\text{cap}} \approx \sigma_{\text{geo}} = \pi \cdot (R_{\text{cl}} + r)^2, \quad (\text{A4})$$

$$\sigma_{\text{cap}} \approx \pi \cdot \left(\left(\frac{3}{4\pi \cdot \rho} \cdot N \right)^{1/3} + r \right)^2. \quad (\text{A5})$$

Here, R_{cl} is the cluster radius, r is the radius of the embedded atom and ρ is the particle density in Ne solids.

While small clusters are formed inside large Ne clusters, Ne atoms are evaporated from the Ne cluster surface (cooling mechanism) and the cluster cross section decreases, respectively, the capture cross section. In a simple model the deposited condensation energy inside Ne clusters as well as the energy due to the evaporation of Ne atoms is proportional to the binding energy per atom E_b of the respective solid. In this picture, Ne \bar{n} clusters doped with 100 Kr atoms evaporate ~ 465 Ne atoms ($E_b(\text{Kr})/E_b(\text{Ne}) \approx 4.65$) and the cluster cross section is, therefore, reduced by roughly 4%. Since this is a rather small effect, we treat the capture cross section as constant and calculate the average size K of the embedded cluster as a function of the cross jet pressure p_Q using Eqs. (A2)–(A6)

$$K(p_Q) = \int_1^\infty k \cdot P_k(L) dk. \quad (\text{A6})$$

¹R. von Pietrowski, M. Rutzen, K. von Haefen, S. Kakar, and T. Möller, *Z. Phys. D: At., Mol. Clusters* **40**, 22 (1997).

²K. von Haefen, T. Laarmann, H. Wabnitz, and T. Möller, *J. Electron Spectrosc. Relat. Phenom.* **106**, 199 (2000).

³T. Laarmann, K. von Haefen, A. Kanaev, H. Wabnitz, and T. Möller, *Phys. Rev. B* **66**, 205407 (2002).

⁴V. A. Apkarian and V. E. Bondybey, *Chem. Phys.* **189**, 137 (1994).

⁵K. Nauta and R. E. Miller, *Science* **283**, 1895 (1999).

⁶K. Nauta and R. E. Miller, *Faraday Discuss.* **113**, 261 (1999).

⁷M. Hartmann, R. E. Miller, J. P. Toennies, and A. Vilesov, *Phys. Rev. Lett.* **75**, 1566 (1995).

⁸N. Schwentner, E. E. Koch, and J. Jortner, *Electronic Excitations in Condensed Rare Gases* (Springer-Verlag, Berlin, 1985).

⁹M. Runne, J. Becker, W. Laasch, D. Varding, G. Zimmerer, M. Liu, and R. E. Johnson, *Nucl. Instrum. Methods Phys. Res. B* **82**, 301 (1993).

¹⁰T. Möller, A. R. B. de Castro, K. von Haefen *et al.*, *J. Electron Spectrosc. Relat. Phenom.* **101**, 185 (1999).

¹¹T. Laarmann, K. von Haefen, H. Wabnitz, and T. Möller, *Surf. Rev. Lett.* **9**, 111 (2002).

¹²O. F. Hagena, *Z. Phys. D: At., Mol. Clusters* **4**, 291 (1987).

¹³U. Buck and R. Krohne, *J. Chem. Phys.* **105**, 5408 (1996).

¹⁴The average Ne cluster size of $\bar{N} = 3500$ given in Ref. 11 was due to an unprecise use of the “scaling laws,” Refs. 12 and 13 (2002).

¹⁵S. Goyal, D. L. Schutt, and G. Scoles, *J. Chem. Phys.* **102**, 2302 (1995).

¹⁶M. Lewerenz, B. Schilling, and J. P. Toennies, *J. Chem. Phys.* **102**, 8191 (1995).

¹⁷I. Fugol, *Adv. Phys.* **27**, 1 (1978).

¹⁸D. R. Miller, *Atomic and molecular beam methods*, Vol. 1 (Oxford University Press, Oxford, New York, 1988).

¹⁹T. Möller and G. Zimmerer, *J. Opt. Soc. Am. B* **6**, 1062 (1989).

²⁰R. Karnbach, Ph.D. thesis, Universität Hamburg (1993).

²¹A. A. Radzig and B. M. Smirnov, *Reference Data on Atoms, Molecules and Ions* (Springer-Verlag, Heidelberg, Berlin, New York, Tokyo, 1985).

²²M. Runne and G. Zimmerer, *Nucl. Instrum. Methods Phys. Res. B* **101**, 156 (1995).

- ²³T. Kloiber and G. Zimmerer, *Phys. Scr.* **41**, 962 (1990).
- ²⁴M. A. Ratner, E. T. Verkhovtseva, and A. M. Ratner, *J. Lumin.* **68**, 255 (1996).
- ²⁵R. Karnbach, M. Joppien, J. Stapelfeld, J. Wörmer, and T. Möller, *Rev. Sci. Instrum.* **64**, 2838 (1993).
- ²⁶S. Petersen, Ph.D. thesis, Universität Hamburg (2000).
- ²⁷F. Holland, K. P. Huber, A. R. Hoy, and R. H. Lipson, *J. Mol. Spectrosc.* **145**, 164 (1991).
- ²⁸A. G. Belov, G. M. Gorbunin, I. Y. Fugol, and E. M. Yurtaeva, *Low Temp. Phys.* **23**, 322 (1997).
- ²⁹M. J. Weber, *Phys. Rev.* **171**, 283 (1968).
- ³⁰L. A. Riseberg and H. W. Moos, *Phys. Rev.* **174**, 429 (1968).
- ³¹G. Zimmerer, *Creation, Motion and Decay of Excitons in Rare-Gas Solids* (U. M. Grassano and N. Terzi, Soc. Italiana di Fisica, Bologna, 1987).
- ³²The size determination of embedded clusters given in Ref. 11 based on an average Ne cluster size of $\bar{N}=3500$, see also Ref. 14 (2002).
- ³³S. Kakar, O. Björneholm, J. Weigelt, A. R. B. de Castro, L. Tröger, R. Frahm, T. Möller, A. Knop, and E. Rühl, *Phys. Rev. Lett.* **78**, 1675 (1997).
- ³⁴M. R. Hoare, *Adv. Chem. Phys.* **40**, 49 (1979).
- ³⁵J. Farges, M. F. de Feraudy, B. Raoult, and G. Torchet, *Surf. Sci.* **106**, 95 (1981).
- ³⁶M. Briant, M. A. Gaveau, J. M. Mestdagh, and J. P. Visticot, *J. Chem. Phys.* **112**, 1744 (2000).
- ³⁷J. Farges, M. F. Feraudy, B. Rault, and G. Torchet, *J. Chem. Phys.* **84**, 3491 (1986).
- ³⁸M. Lewerenz, B. Schilling, and J. P. Toennies, *J. Chem. Phys.* **106**, 5787 (1997).